Article:
Dawson, J F, Austin, A N, Flintoft, I D et al. (2017) Shielding Effectiveness and Sheet Conductance of Nonwoven Carbon-Fiber Sheets. IEEE Transactions on Electromagnetic Compatibility. 7565608. pp. 84-92. ISSN: 0018-9375

https://doi.org/10.1109/TEMC.2016.2601658

Shielding Effectiveness and Sheet Conductance of Nonwoven Carbon-fibre Sheets

John F. Dawson[1], Andrew N. Austin[2], Ian D. Flintoft[1] and Andy C. Marvin[1]

[1]*Department of Electronics, University of York, Heslington, York YO10 5DD, UK*
[2] *Technical Fibre Products Ltd, Burneside Mills, Kendal, LA9 6PZ, UK.*

Published in IEEE Transactions on Electromagnetic Compatibility, vol. 59, no. 1, pp. 84-92, 2017.

Accepted for publication 04/08/2016.

DOI: 10.1109/TEMC.2016.2601658

Shielding Effectiveness and Sheet Conductance of Nonwoven Carbon-fibre Sheets

John F. Dawson, *Member, IEEE,* Andrew N. Austin, *Member, IEEE,* Ian D. Flintoft, *Senior Member, IEEE* and Andrew C. Marvin, *Fellow, IEEE*

***Abstract*—Nonwoven carbon-fibre sheets are often used to form a conductive layer in composite materials for electromagnetic shielding and other purposes. While a large amount of research has considered the properties of similar idealised materials near the percolation threshold, little has been done to provide validated analytic models suitable for materials of practical use for electromagnetic shielding. Since numerical models consume considerable computer resource, and do not provide the insight which enables improved material design, an analytic model is of great utility for materials development. This paper introduces a new theoretical model for the sheet conductance of nonwoven carbon-fibre sheets built on the theory of percolation for two-dimensional conducting stick networks. The model accounts for the effects of sample thickness, fibre angle distribution and contact conductance on the sheet conductance. The theory shows good agreement with Monte-Carlo simulations and measurements of real materials in the supercritical percolation regime where the dimensionless areal concentration of fibres exceeds about 50. The theoretical model allows the rapid prediction of material shielding performance from a limited number of manufacturing parameters.**

***Index Terms*—electromagnetic shielding effectiveness, percolation theory, sheet conductance, carbon fibre composite, nonwoven fabric**

I. Introduction

A nonwoven fabric is an array of fibres that are formed into a sheet using a wet-laid process like that used for paper manufacture. Nonwoven materials possess a complicated structure with varying local parameters such as thickness, areal density, and fibre angle. Fig. 1 shows a scanning electron microscope (SEM) image of a nonwoven fabric, constructed from 12 mm long polyacrylonitrile carbon fibres, 7 μm in diameter, stabilised using a polyester binder.

Nonwoven materials are used throughout the aerospace, defence and medical industries, usually to provide lightweight, functional enhancement to existing composite structures. Applications include electromagnetic shielding, collapsible antenna reflectors and defibrillator electrodes. We have observed that the shielding effectiveness of the nonwoven materials we have available varies very little with frequency up to several gigahertz (see Fig. 2), and therefore depends principally on the sheet conductance [1].

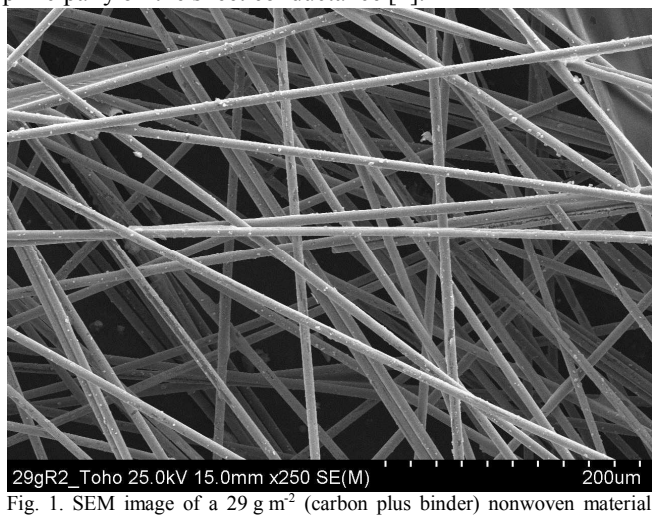

Fig. 1. SEM image of a 29 g m^{-2} (carbon plus binder) nonwoven material constructed of carbon fibres.

A large body of work on percolation in two- and three-dimensional conducting stick networks has been reported following from the founding work of Balberg and Binenbaum [2]. Much of this work has focused on the behavior of the material, including its homogenised sheet conductance near the percolation threshold. Practical shielding materials typically have fibre concentrations far above the percolation threshold; more recent work has begun to study this regime using Monte Carlo simulation [3–5]. The effects of fibre angle distribution [6] and contact conductance [7] on the conductivity have also been studied. However, there is a lack of directly applicable analytical or semi-empirical models for accurate prediction of sheet conductance, and therefore shielding effectiveness, which incorporates all these effects at high concentrations. This paper describes a method of determining the sheet conductance based on a semi-analytic formulation and compares it against results obtained using both Monte Carlo models of the material and measurements on a range of real materials.

II. Measurement of Nonwoven Sheets

A. Shielding effectiveness measurement

The shielding effectiveness of six carbon fibre veil samples of differing areal density were measured in both *x*- and *y*-

Submitted for review xxth February 2016. This work was supported by Technical Fibre Products Ltd, Kendal, UK.

J. F. Dawson, I. D. Flintoft, and A. C. Marvin are with the Department of Electronics, University of York, Heslington, York, YO10 5DD (e-mail: {ian.flintoft, andy.marvin, john.dawson}@york.ac.uk).

A. N. Austin is with Technical Fibre Products Ltd, Burneside Mills, Kendal, LA9 6PZ, UK. (e-mail: andrew.austin@tfpglobal.com).

polarisations using the method described in [8]. For three of the samples Fig. 2 shows the measured SE (lines) and the result of fitting Shelkunoff's theory [9] to the measured data between 1 and 2.5 GHz (points). The sheet conductance was determined from the fitted curve and is compared with the results predicted by the Monte Carlo models (MCMs) below. Note that Fig. 2 and other figures in this paper show the areal density of the carbon fibre in the veil only and do not include the density of the binder. With binder the nominal areal densities of the veils used are 4, 10, 17, 34, 50 and 75 g m^{-2} which contain 3.1, 8.2, 14.8, 30.5, 43.6, and 56.1 g m^{-2} of carbon fibre respectively, based on measurements of the sample weights after the binder was removed by heating. In our earlier papers [1,10,11] only the nominal density is reported.

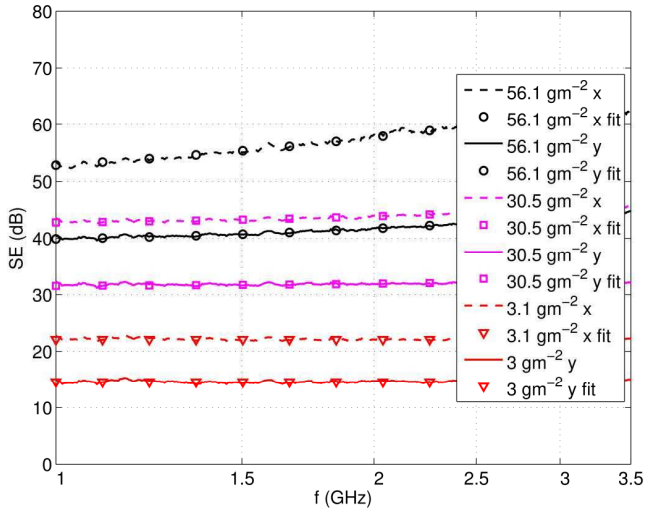

Fig. 2. Measured shielding effectiveness (lines) and Schelkunoff fit between 1 and 2.5 GHz (points) in two polarisations for three of the veil samples.

B. *Sheet conductance measurements*

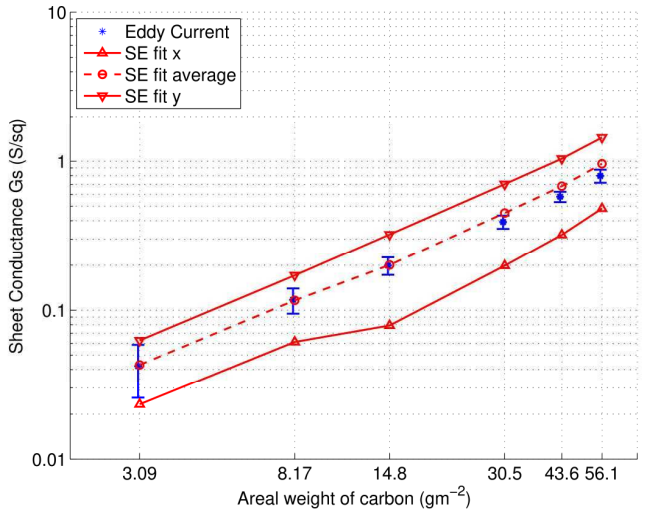

Fig. 3. The sheet conductance deduced from the shielding effectiveness measurement for each polarisation. The average is compared with the average of that measured on 18 samples with an eddy current probe with error bars at three standard deviations.

The sheet conductance deduced from the shielding effectiveness measurements is shown in Fig. 3. The average of the conductance obtained in each of the two polarisations from the shielding measurement is also compared with averages taken at 18 positions with an eddy-current probe. The eddy current probe measures over a 25 mm diameter circle and revealed considerable sample variation from point to point. For the SE measurement the values are effectively averaged over the area (140 mm × 150 mm) of the shielding sample.

C. *Thickness measurements*

The thicknesses of five samples of each available areal density of the carbon fibre nonwoven sheets were measured, using a micrometer with 2 kPa pressure applied. The average at each density was then fitted to the function

$$t = t_{min} \sqrt[\alpha]{1 + \left(\frac{\rho_A}{\rho_{A0}}\right)^{\alpha}} \quad (1)$$

where t is the thickness of the veil, defined as the distance between the centres of the outermost fibres (that is, one fibre diameter less than the distance between the outer surfaces of the fibres). We chose this measure of thickness as it fits with the way the MCM veils are generated and seems to give a better result in the later analysis than the thickness measured to the outer surface of the veil. t_{min}, is the minimum thickness of the veil, ρ_A is the areal density of the carbon fibre content of the veil, ρ_{A0} is the areal density at which the thickness of the veil transitions from constant thickness to a thickness proportional to the areal density. The parameter $\alpha = 2$ determines the shape of the curve in the transition region. In practice, the 3 g m^{-2} areal density is the lightest material manufactured so the shape of the curve below this density is likely to be inaccurate. However, we expect the thickness to approach that of the fibre diameter as the areal density is reduced, and it is useful to define a feasible thickness so that the possible material behaviour at lower areal densities can be studied using the MCM.

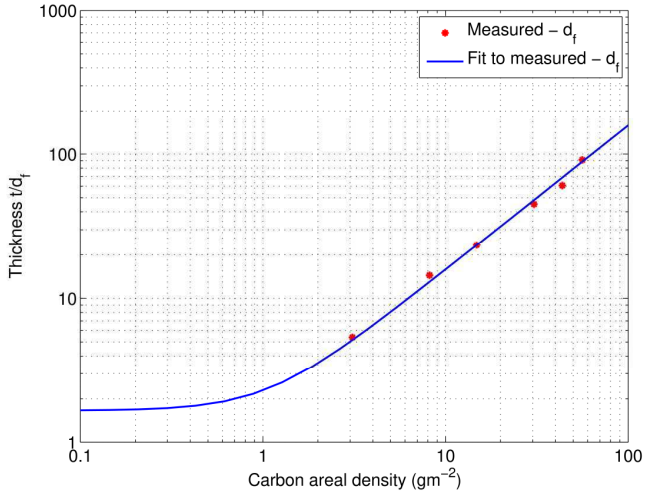

Fig. 4. Measured thickness of the real nonwoven sheets and fitted thickness function.

III. Sheet Conductance of a Fibre Network

Here we derive an approximate, average solution for the conductance of an anisotropic sheet network of randomly organised fibres, and with the aid of previous work on 2D

isotropic networks and MCM simulations, we generalise it to the case of 3D sheets including the effect of contact conductance between the fibres. The concentration of fibres is assumed to be sufficiently large that each fibre is well connected to its neighbours. The formulation does not work for low areal densities where fibres may only be partially connected.

A. Sheet conductance in the absence of contact conductance

Consider a single path, n, through a square area of veil material of side length l_s with the conducting fibres at a fixed angle from the direction of the average current flow, as shown in Fig. 5. If l_s is the same as the fibre length, the conductance of the square in the *x*-direction, due to the fibre conductivity is

$$G_{\text{fsx,n,1}} = \text{G}_f \cos\varphi_{f,n} \tag{2}$$

where G_f is the conductance of the fibre and $\varphi_{f,n}$ is the angle of the fibre(s) in path n from the *x*-axis. If the fibres composing the path are assumed to be of length l_s, then the number of fibres required to make the path is

$$\tilde{n}_{A,n,1} = \frac{1}{\cos\varphi_{f,n}} \tag{3}$$

and $\tilde{n}_{A,n,1}$ is the number of fibres for one path in an area equal to the square of the fibre length (l_f), which is a dimensionless measure of the areal density of the material. Combining (2) and (3) we get:

$$G_{\text{fsx,n,1}} = \tilde{n}_{A,n}\text{G}_f \cos^2\varphi_{f,n} \tag{4}$$

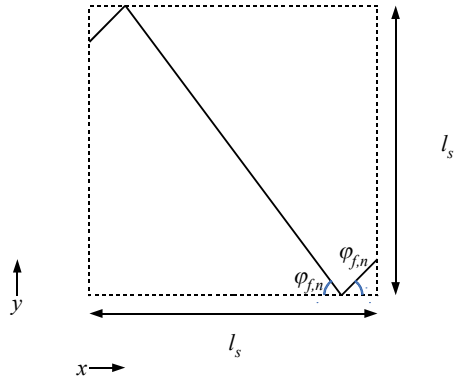

Fig. 5. A single conducting fibre path at angle φ_f to the x-directed current flow in a material sample of size $l_s$square.

If a number of paths, $N_{P,n}$ are present at each possible angle, $\varphi_{f,n}$, then the conductivities of each path can be added so that the conductance of the square becomes

$$G_{\text{fsx}} = \text{G}_f \sum_{n=1}^{N_\varphi} N_{P,n}\tilde{n}_{A,n,1}\cos^2\varphi_{f,1} \tag{5}$$

where the number of path angles is N_φ. If we consider that the total areal density of the square is the sum of the individual path densities then we have

$$\tilde{n}_A = \sum_{n=1}^{N_\varphi} N_{P,n}\tilde{n}_{A,n,1} \tag{6}$$

Further, if the proportion of the total density contributed by each path at angle $\varphi_{f,n}$ is

$$P(\varphi_{f,n}) = \frac{N_{P,n}\tilde{n}_{A,n,1}}{\tilde{n}_A} \tag{7}$$

then we could write (5) as

$$G_{\text{fsx}} = \text{G}_f \tilde{n}_A \sum_{n=1}^{N_\varphi} P(\varphi_{f,n})\cos^2\varphi_{f,n} \tag{8}$$

where N_φ is the number of fibre angles. The summation is purely a function of the proportion of the paths at each angle and we therefore define the geometry factor

$$\Phi_x = \sum_{n=1}^{N_\varphi} P(\varphi_{f,n})\cos^2\varphi_{f,n} \approx \int_{\frac{-\pi}{2}}^{\frac{\pi}{2}} p(\varphi_f)\cos^2\varphi_f d\varphi_f \tag{9}$$

where $p(\varphi_f)$ is the angular probability density function (PDF) of the fibre distribution in the material [6]. The sheet conductance in the *x*-direction is therefore

$$G_{\text{fsx}} = \text{G}_f \tilde{n}_A \Phi_x \tag{10}$$

Similarly the sheet conductance in the orthogonal *y*-direction is

$$G_{\text{fsy}} = \text{G}_f \tilde{n}_A \Phi_y \tag{11}$$

where

$$\Phi_y = \sum_{n=1}^{N_\varphi} P(\varphi_{f,n})\sin^2\varphi_{f,n} \approx \int_{\frac{-\pi}{2}}^{\frac{\pi}{2}} p(\varphi_f)\sin^2\varphi_f d\varphi_f \tag{12}$$

and we note that $\Phi_x + \Phi_y = 1$.

B. Effect of contact conductance

As current crosses between fibres it must pass through any contact conductance [7]. If we begin with a material where there is one contact conductance, G_c, at each end of a fibre forming a path, then the number of contact conductances in series traversed as the current passes through one square of material with sides equal to the fibre length, on a single path at angle $\varphi_{f,n}$ must be

$$N_{scx,n,1} = \frac{1}{cos\varphi_{f,n}} = \tilde{n}_{A,n,1} \tag{13}$$

and there are $\tilde{n}_{A,n,1}$ fibres in the unit area equal to the square of the fibre length due to the single path as in (3). The conductance per unit square due to contact conductance in the *x*-direction due to one path, if each fibre only contributes one contact, is therefore

$$G_{csx,n,1} = \frac{G_c}{N_{scx,n,1}} = G_c cos\varphi_{f,n} \tag{14}$$

If a number of parallel paths, $N_{P,n}$, exist at the same angle, $\varphi_{f,n}$, then the conductances can be added

$$G_{csx,n} = N_{P,n}G_c cos\varphi_{f,1} \tag{15}$$

and the number of fibres per unit area will be

$$\tilde{n}_{A,n} = N_P\tilde{n}_{A,n,1} \tag{16}$$

Using (16) and (13) we can rewrite (15) as

$$G_{csx,\text{n}} = \frac{\tilde{n}_{A,n}}{\tilde{n}_{A,1}} G_c cos\varphi_{f,\text{n}} = \tilde{n}_{A,n}G_c cos^2\varphi_{f,1} \tag{17}$$

For a material with a number, N_φ, of sets of paths at different angles, the conductances of the individual sets of paths can be summed to give the overall conductance, due to contact conductance, per unit square

$$G_{csx} = G_c \sum_{n=1}^{N_\varphi} \tilde{n}_{A,n} cos^2\varphi_{f,n} \tag{18}$$

This can be manipulated in the same way as (7)-(12) so that the contact conductances per square in the *x*- and *y*-directions are

$$G_{csx} = G_c\tilde{n}_A\Phi_x \tag{19}$$

and

$$G_{csy} = G_c\tilde{n}_A\Phi_y \tag{20}$$

In practice there are more contacts per fibre as overlapping fibres touch. If the actual number of contacts per fibre is N_{cf}, then that will add additional parallel paths such that [12]

$$G_{csx} = \frac{k_e N_{cf}}{2} G_c \tilde{n}_A \Phi_x \quad (21)$$

The factor of two appears as half the contacts may be considered to allow current to flow on to the fibre and half allow it to flow off. The effectiveness of each contact depends on the potential difference between the two fibres and k_e is a factor which allows for this effect. By equating the coefficients in our result with those of Žeželj and Stanković [13] for a uniform 2D fibre angular distribution we find $k_e = 0.1696$. We determine the number of contacts per fibre in Section IV.C.

C. *Overall sheet conductance*

The overall sheet conductance per square is equal to the series combination of the conductance due to the fibres and the contacts:

$$G_s = \frac{1}{\frac{1}{G_{fs}} + \frac{1}{G_{cs}}} \quad (22)$$

IV. Monte Carlo Modelling of Nonwoven Sheets

A. *Generation of the Monte Carlo model*

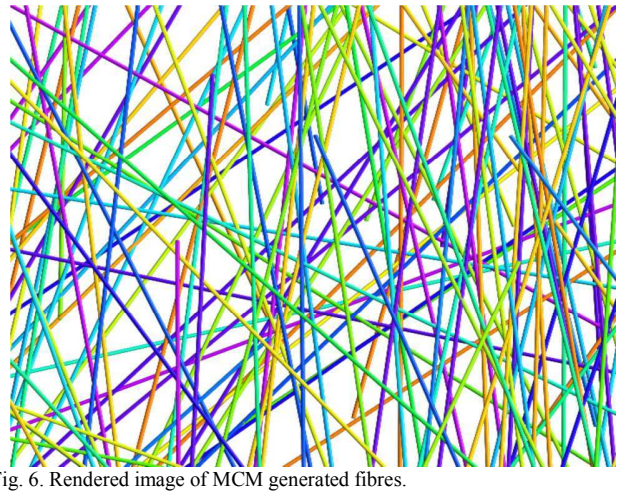

Fig. 6. Rendered image of MCM generated fibres.

A Monte Carlo simulator was written to generate fibres of a given length, l_f, and diameter, d_f, in random positions and orientations within a defined sheet volume [1,14]. The position of the centre of the axis of each fibre is chosen uniformly within the volume, and a rotation angle, $\varphi_{f,n}$, in the x-y plane, is chosen for each fibre according to a selected PDF, $p(\varphi_f)$. The fibre is then rotated through a uniformly random angle of elevation, $\theta_{f,n}$, which is constrained to keep the fibre ends within the thickness, t, of the material. Any fibres crossing the transverse boundaries of the volume are truncated, and the truncation points at the edges will form connections to the sheet. Pairs of fibres with an axial distance of less than d_f between them are deemed to be connected. Using the connections between fibres, a resistor network is defined by a nodal admittance matrix. The admittance matrix can be solved to determine the conductance of the sheet in the x and y directions [15]. The sheet conductances are averaged over a number of simulations to determine the average value.

Fig. 7 compares the results of the MCM with the theory developed here, and the expression given by Žeželj and Stanković [13] for a 2D isotropic sheet with infinite contact conductance. In Figs. 7-10,13,15, and 16 the sheet conductance is normalised to the fibre conductance to allow simple comparison with [13]. For the MCM the mean x- and y-directed conductivities over a number of simulations are shown along with bars at one standard deviation. At low values of $\tilde{n}_A$ the conductivity falls below that predicted in this paper as the proportion of fibres that are connected falls. Also the variability of the model increases with decreasing $\tilde{n}_A$, though the average agrees well with Žeželj and Stanković. As expected the theory presented here works well for $\tilde{n}_A > 50$ where the fibres are well connected. This is below the minimum concentration which can be manufactured for the carbon fibre veils measured in this paper.

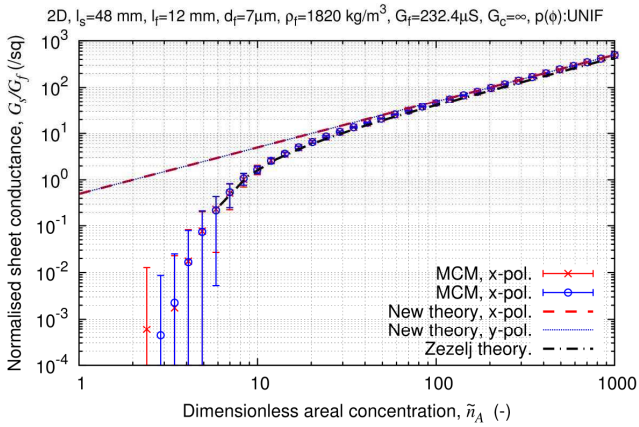

Fig. 7. Normalised sheet conductance of a 2D isotropic veil (with a uniform angular distribution), with 232.4 µS fibre and infinite contact conductance, generated by the MCM and compared with the analytic expressions.

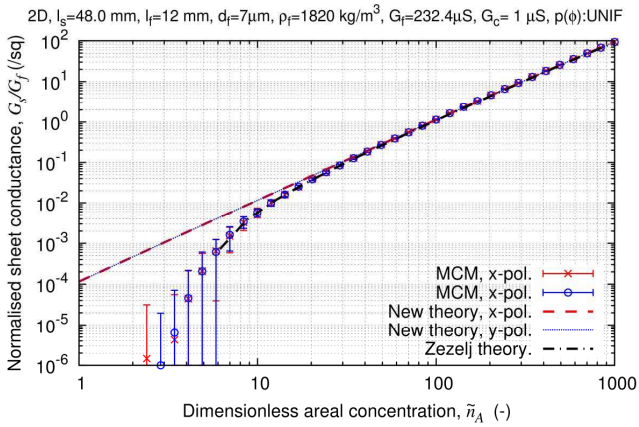

Fig. 8. Normalised sheet conductance of a 2D isotropic veil (with a uniform angular distribution), with 232.4 µS fibre and 1 µS contact conductance, generated by the MCM and compared with the analytic expressions.

In Fig. 8 a 1 µS contact conductance is added so that the behaviour of the material is dominated by the contact conductance. It can be seen here that the sheet conductance varies with the square of the fibre concentration as expected from (21) and (25). Again our formulation shows good correspondence with the MCM for $\tilde{n}_A > 50$, and the MCM model corresponds closely to that predicted by Žeželj, &

Stanković.

In Fig. 9, a 100 µS contact conductance is used so that the behaviour of the material at low concentrations is dominated by the contact conductance, but at higher concentrations the fibre conductance dominates. Again the MCM shows results which closely follow that predicted by Žeželj and Stanković and our formulation works well for $\tilde{n}_A > 50$.

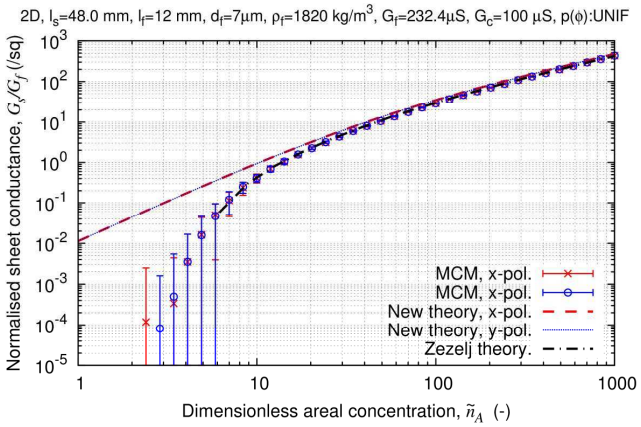

Fig. 9. Normalised sheet conductance of a 2D isotropic veil (with a uniform angular distribution), with 232.4 µS fibre conductance and 100 µS contact conductance, generated by the MCM and compared with the analytic expressions.

B. *Effect of anisotropy on sheet conductance due to fibres*

In order to verify the analytic solution (8), derived above, sheets with infinite contact conductance and a truncated Gaussian PDF of fibre angles were simulated using MCMs.

Fig. 10 shows the sheet conductance for the case with infinite contact conductance and a truncated Gaussian fibre angle PDF with scale parameter $\sigma = 30$ deg and zero mean. For this distribution $\Phi_x = 0.79$ and $\Phi_y = 0.21$. It can be seen that the analysis presented here corresponds well to the MCM for areal concentrations $\tilde{n}_A > 50$. The formulation of Žeželj and Stanković has no mechanism to include the effects of anisotropy and so we plot only the curve for an isotropic material in Fig. 10 for comparison.

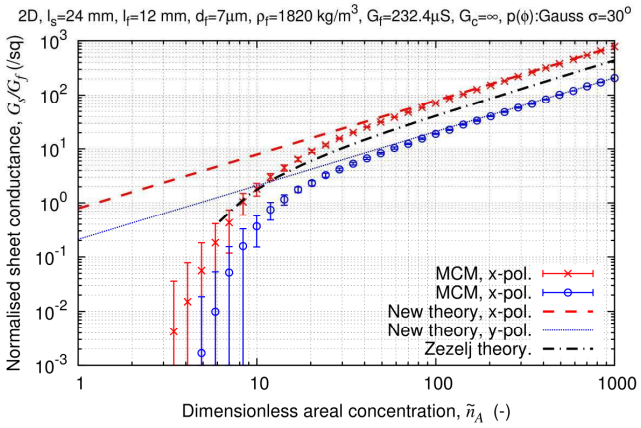

Fig. 10. Normalised sheet conductance of a 2D anisotropic veil with a truncated Gaussian angular distribution with zero mean and $\sigma = 30$ deg, with 232.4 µS fibre and infinite contact conductance. The MCM is compared with the analytic solutions from this paper and empirical expression of Žeželj and Stanković.

C. *Effect of anisotropy on the number of contacts per fibre*

The number of contacts per fibre predicted by the MCM for a 2D material with truncated Gaussian, non–uniform, angular distributions were compared with the value predicted by Heitz [16] for a uniform angular fibre distribution. For a uniform angular PDF, Heitz's theory fits closely to the MCM results, and for truncated Gaussian PDFs the number of contacts is reduced though it is still proportional to the fibre concentration.

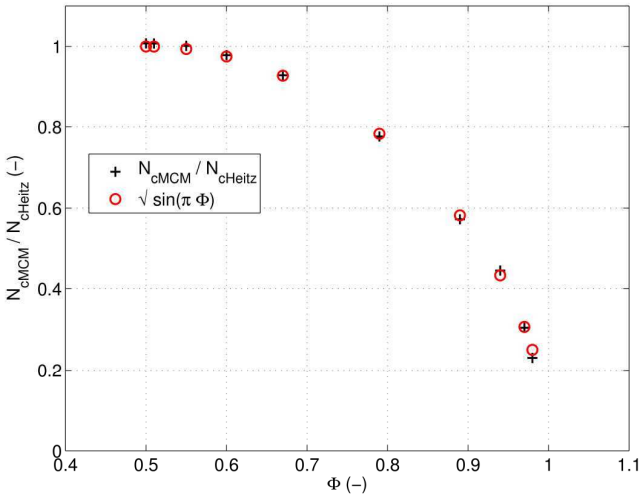

Fig. 11. Comparing the number of contacts per fibre predicted by Heitz for a uniform 2D sheet with 2D MCM sheets with Gaussian angular PDFs, and the empirical estimate which has an RMS error of 1 % from the MCM and maximum error of 8.7 % in the magnitude at the largest Φ value. The standard deviation of the MCM results is approximately the same size as the markers so is not shown.

D. *Effect of thickness on the number of contacts per fibre*

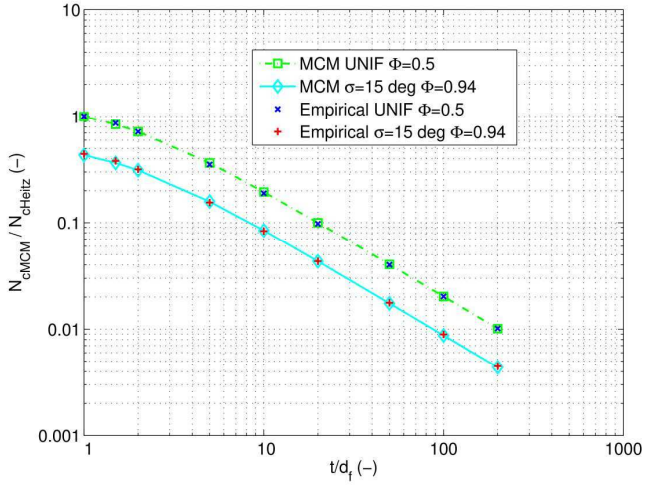

Fig. 12. Comparing the number of contacts per fibre predicted by Heitz for a uniform 2D sheet with 3D MCM sheets with uniform and $\sigma = 15$ deg zero mean, truncated Gaussian angular PDFs and the empirical estimate.

Fig. 11 shows the variation in number of contacts per fibre versus the geometry factor, Φ. It was found that a good approximation to the behaviour was given by

$$\frac{N_{\mathrm{cMCM}}}{N_{\mathrm{cHeitz}}} = \sqrt{\sin(\pi\Phi)} \qquad (23)$$

where $N_{\mathrm{cHeitz}} = P_{cont}\pi\tilde{n}_A$ is the number of contacts predicted

by Heitz, and N_{cMCM} is the number of contacts predicted by the MCM.

The effect of thickness on the number of contacts per fibre was compared with the prediction of Heitz for the 2D uniform angular distribution, and truncated Gaussian angular distributions using the MCM. It can be seen in Fig. 12, that the number of contacts per fibre reduces compared with the 2D case, as the material thickness increases.

Taking into account the change in number of contacts due to the non-uniform distribution of fibre angles according to (23) a simple relationship was found to provide a good fit to the effect of thickness for 3D anisotropic samples:

$$\frac{N_{\mathrm{cMCM}}}{N_{\mathrm{cHeitz}}} = \sqrt{\sin(\pi\Phi)}^{1.5}\sqrt{\frac{1+(0.66)^{1.5}}{1+(0.66\tilde{t})^{1.5}}} \tag{24}$$

Here $\tilde{t} = t/d_f$ is the material thickness in fibre diameters, where t is defined as the distance between the centres of the outermost fibres. This relationship is based partly on how the thickness is defined in the MCM, but it also seems to provide a better fit than using the outer part of the fibre as the measure of thickness. Note (24) is valid only for $\tilde{t} \geq 1$. For $\tilde{t} \leq 1$, the material is effectively two-dimensional as the centre lines of any fibres crossing in the *x*-*y* plane will always lie within one fibre diameter of each other. The behaviour of the 2D material is then as given in (23).

So overall the number of contacts per fibre is given by

$$N_{cf} = P_{cont}\pi\tilde{n}_A\sqrt{sin(\pi\Phi_x)}^{1.5}\sqrt{\frac{1+(0.66)^{1.5}}{1+(0.66\tilde{t})^{1.5}}} \tag{25}$$

where $P_{\mathrm{cont}} = 0.2027$ [16]. In practical materials the thickness increases with fibre concentration and it is therefore important to know this relationship if the effect of contact conductance is to be predicted.

E. Comparison of 3D Monte Carlo and analytic results

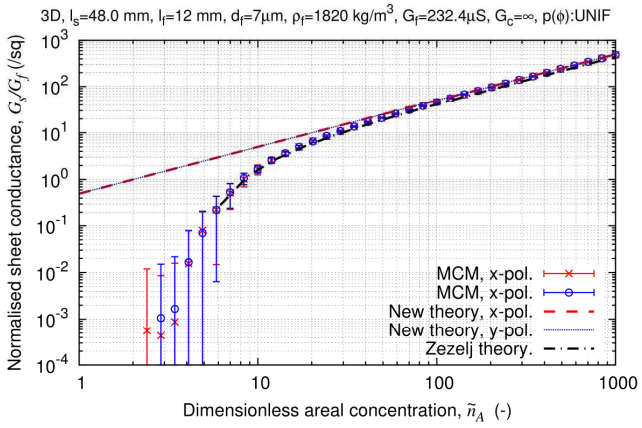

Fig. 13. Normalised sheet conductance of a 3D isotropic veil with a uniform angular distribution, with 232.4 µS fibre and infinite contact conductance, generated by the MCM and compared with the analytic solutions from this paper and empirical expression of Žeželj and Stanković.

In Fig. 13 it can be seen that the MCM, analytic solutions from this paper and empirical expression of Žeželj Stanković correspond well in the 3D case for a uniform fibre angular distribution. This is as expected since for infinite contact conductance the 2D and 3D behaviours are identical as long as each fibre is well connected. The material has a thickness which is defined by the function

$$\tilde{t} = \sqrt{1 + 0.00667\tilde{n}_A^2} \tag{26}$$

which is comparable to the real nonwoven veils that we measured. It can be seen in Fig. 14 that the number of contacts per fibre levels off for areal concentrations $\tilde{n}_A > 100$ which will affect the conductivity of any veil with finite contact conductance, compared to the 2D case.

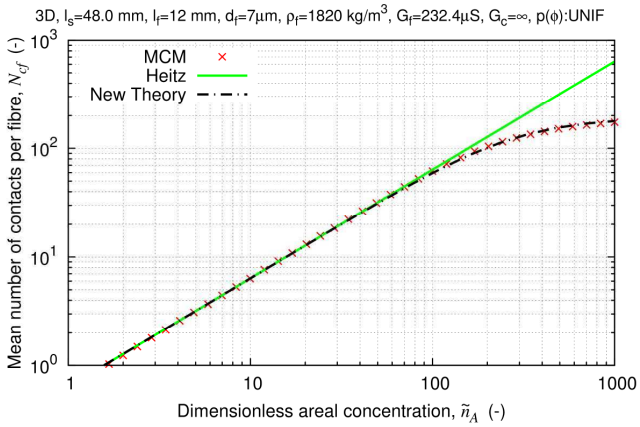

Fig. 14. Number of contacts per fibre for a 3D isotropic veil with a uniform angular distribution, comparing the MCM, as predicted by (25) and the 2D theory of Heitz [5].

Fig. 15 shows the conductivity for a similar 3D isotropic veil with 1 µS contact conductance. The number of contacts per fibre is the same as in Fig. 14. It can be seen that the reduction in contacts per fibre, below that predicted by the 2D theory, results in a reduction in sheet conductance for areal concentrations $\tilde{n}_A > 50$ compared with the 2D theory. The MCM and the model presented in this paper agree closely in this region.

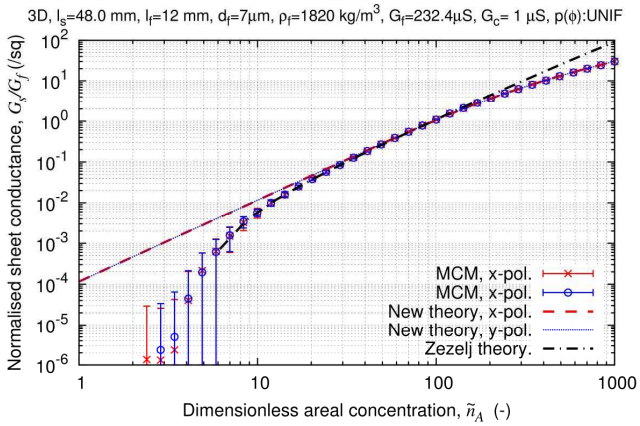

Fig. 15. Normalised sheet conductance of a 3D isotropic veil with a uniform angular distribution, with 232.4 µS fibre and 1 µS contact conductance, generated by the MCM and compared with the analytic solutions from this paper and empirical expression of Žeželj, & Stanković.

Fig. 16 shows the conductivity of a 3D isotropic veil with a truncated Gaussian angular distribution with zero mean and $\sigma = 30$ deg. Again it can be seen that the MCM and theory presented in this paper agree well for $\tilde{n}_A > 50$. The 2D empirical expression of Žeželj and Stanković does not include the effects of a non-uniform angular distribution or veil thickness and is included here for reference. It can be seen in

Fig. 17 that the number of contacts per fibre levels off for areal concentrations $\tilde{n}_A > 100$ and also sits below the 2D approximation of Heitz for lower concentrations, both of which will affect the conductivity of any veil with finite contact conductance, compared to the 2D case.

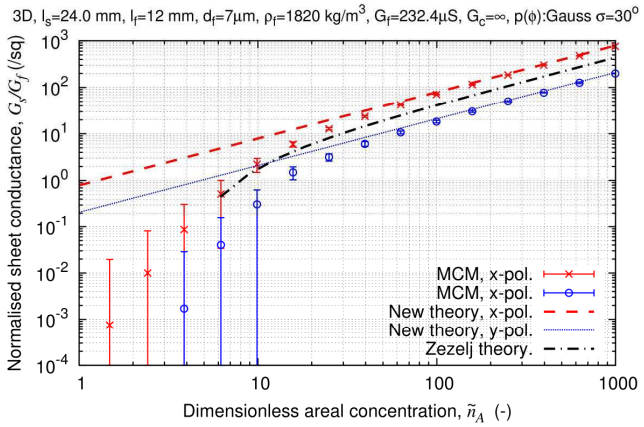

Fig. 16. Normalised sheet conductance of a 3D veil with a truncated Gaussian angular distribution with zero mean and $\sigma = 30$ deg., giving $\Phi_x = 0.79$ and $\Phi_x = 0.21$, with 232.4 µS fibre and infinite contact conductance, comparing MCM, analytic solutions from this paper and empirical expression of Žeželj and Stanković.

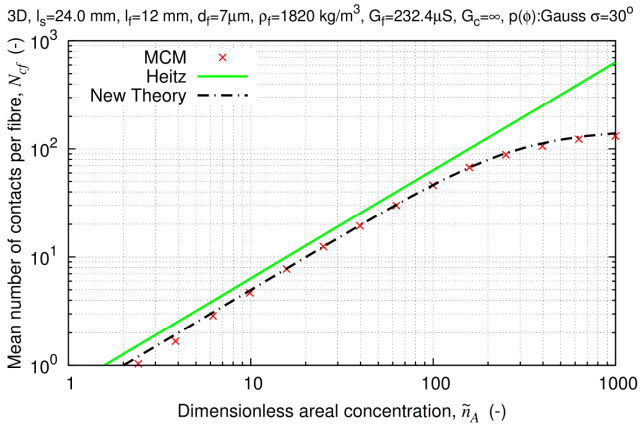

Fig. 17. Number of contacts per fibre for a 3D veil with a truncated Gaussian angular distribution with zero mean and $\sigma = 30$ deg., comparing the MCM, as predicted by (24) compared with the 2D theory of Heitz [5].

F. Modelling real materials

In order to determine the fibre angle distribution in real nonwoven materials a Hough transform was performed on 50 images of each of two materials to determine the position and angle of each fibre as described in [1]. This was only possible on the 4 g m^{-2} and 10 g m^{-2} materials where the optical density was low enough to allow individual fibres to be distinguished. Fig. 18 shows the PDFs obtained, which are similar for both densities. The measured PDF from the 10 g m^{-2} material, along with the thickness function determined in Section II.C was then used to generate 3D MCMs comparable with the range of real materials available.

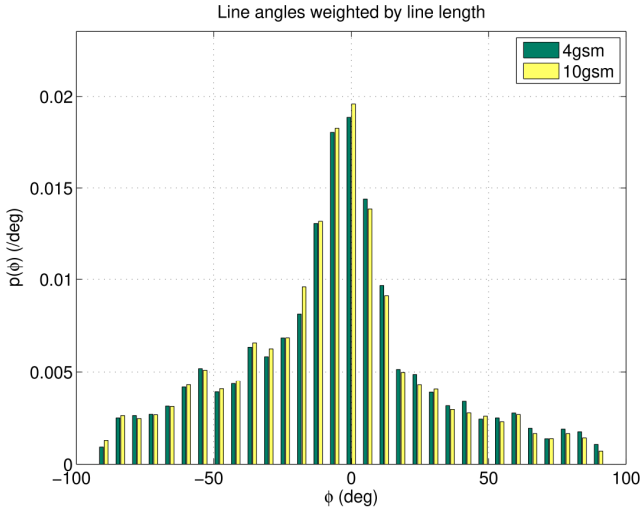

Fig. 18. Histogram of the fibre angle distribution for 4 g m^{-2} ($\Phi_x = 0.725$) and 10 g m^{-2} ($\Phi_x = 0.731$) nonwoven materials.

First a material with infinite contact conductance was modelled. In Fig. 19 it can be seen that the analytic and MCM results match well but that the measured data shows a lower conductance. This is presumed to be due to finite contact conductance.

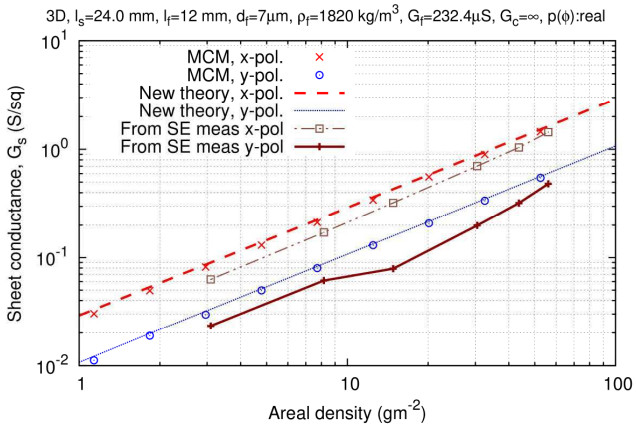

Fig. 19. Sheet conductance of real nonwoven material compared with MCM and analytical result, with 232.4 µS fibre and infinite contact conductance.

Using the results from Fig. 19 and our theory we estimated that a 116.65 µS contact conductance would give a good fit between the MCM and the measured data. In Fig. 20 we show the results with this contact conductance, which brings the MCM prediction close to the measured data. It can be seen here that the analytic result corresponds less well to the MCM and measured solutions. This may be due to the different form of the fibre angular distribution than used in our initial tests. The number of contacts per fibre predicted by the theory corresponds well with the MCM so this can be eliminated as the cause of the discrepancy.

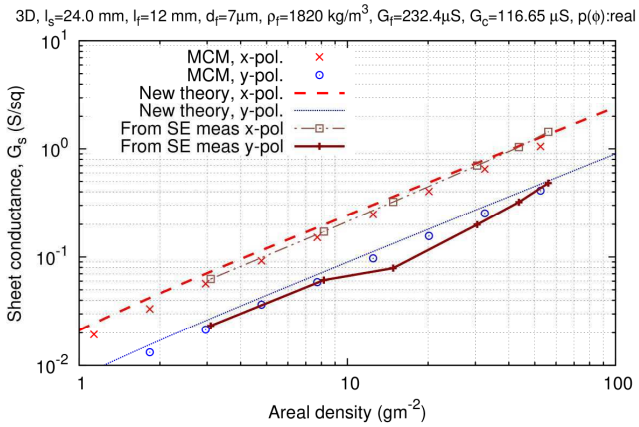

Fig. 20. Sheet conductance of real nonwoven material compared with MCM and analytical result, with 232.4 μS fibre and 116.65 μS contact conductance.

V. Conclusions

We have presented a new theoretical model for efficiently determining the sheet conductance of 2D and 3D anisotropic nonwoven sheet materials which includes the effect of both fibre and contact conductance. We have used empirical approximations to extend the model to include the effect of contact conductance with anisotropic materials. The model shows a good agreement with Monte Carlo models using both uniform and Gaussian fibre angular distributions for materials which have areal concentrations well above the percolation threshold such as those which can be practically manufactured. We have compared the model with real nonwoven materials and found the model to give good correspondence with the measurements, but with a slightly reduced accuracy regarding the behaviour of contact conductance. We postulate this is due to the dependence of the effectiveness of the contacts being variable with the fibre angle distribution. The ability to predict the sheet conductance of nonwoven sheets allows the shielding effectiveness of practical materials to be estimated over a wide range of frequencies for practical materials, though our current model does not include the effect of skin depth in the material so becomes less accurate at higher frequencies where this is significant.

As well as enabling the design of conductive nonwoven materials, and insight into the factors which determine their performance, the results presented here also have applications to the broader range of problems where conductive fibres are embedded in sheet materials, and allow the behaviour to be calculated in seconds. Typically the Monte Carlo models, implemented in MATLAB, take several hours to run.

References

[1] A.N. Austin, J.F. Dawson, I.D. Flintoft, and A.C. Marvin, "Modelling the micro-structure of non-uniform conductive non-woven fabrics: Determination of sheet resistance," *Electromagnetic Compatibility (EMC Europe), 2015 International Symposium on*, Dresden, Germany: 2015, pp. 1–6.

[2] I. Balberg and N. Binenbaum, "Computer study of the percolation threshold in a two-dimensional anisotropic system of conducting sticks," *Physical Review B*, vol. 28, Oct. 1983, p. 3799.

[3] J. Li and M. Östling, "Conductivity scaling in supercritical percolation of nanoparticles–not a power law," *Nanoscale*, vol. 7, 2015, pp. 3424–3428.

[4] R.M. Mutiso, M.C. Sherrott, A.R. Rathmell, B.J. Wiley, and K.I. Winey, "Integrating simulations and experiments to predict sheet resistance and optical transmittance in nanowire films for transparent conductors," *ACS Nano*, vol. 7, Aug. 2013, pp. 7654–7663.

[5] R.M. Mutiso and K.I. Winey, "Electrical percolation in quasi-two-dimensional metal nanowire networks for transparent conductors," *Physical Review E*, vol. 88, Sep. 2013, p. 032134.

[6] F. Du, J.E. Fischer, and K.I. Winey, "Effect of nanotube alignment on percolation conductivity in carbon nanotube/polymer composites," *Physical Review B*, vol. 72, Sep. 2005, p. 121404(R).

[7] P. Keblinski and F. Cleri, "Contact resistance in percolating networks," *Physical Review B*, vol. 69, May. 2004, p. 184201.

[8] A.C. Marvin, L. Dawson, I.D. Flintoft, and J.F. Dawson, "A Method for the Measurement of Shielding Effectiveness of Planar Samples Requiring No Sample Edge Preparation or Contact," *IEEE Transactions on Electromagnetic Compatibility*, vol. 51, May. 2009, pp. 255–262.

[9] S.A. Schelkunoff, "The impedance concept and its application to problems of reflection, refraction, shielding, and power absorption," *Bell System Tech. J.*, vol. 17, 1938, pp. 17–48.

[10] A.N. Austin, J.F. Dawson, and A. Marvin, "Analysis of the shielding properties of metalized nonwoven materials," *EuroEM 2012*, 2012.

[11] A.N. Austin, J.F. Dawson, I.D. Flintoft, and A.C. Marvin, "Analysis of the shielding properties of metalised nonwoven materials," *Electromagnetic Compatibility (EMC EUROPE), 2013 International Symposium on*, Bruges, Belgium: 2013, pp. 526–531.

[12] G. Ruschau, S. Yoshikawa, and R. Newnham, "Resistivities of conductive composites," *Journal of Applied Physics*, vol. 72, Aug. 1992, pp. 953–959.

[13] M. Žeželj and I. Stanković, "From percolating to dense random stick networks: Conductivity model investigation," *Physical Review B*, vol. 86, Oct. 2012.

[14] M.E. Newman and R.M. Ziff, "Fast Monte Carlo algorithm for site or bond percolation," *Physical Review E*, vol. 64, Jun. 2001, p. 016706.

[15] J. Rommes and W.H. Schilders, "Efficient methods for large resistor networks," *IEEE Ttransactions on Computer-aided Design of Integrated Circuits and Systems*, vol. 29, Jan. 2010, pp. 28–39.

[16] J. Heitz, Y. Leroy, L. Hebrard, and C. Lallement, "Theoretical characterization of the topology of connected carbon nanotubes in random networks," *Nanotechnology*, vol. 22, Jul. 2011, p. 345703.